

# $P$ -wave states $T_{bb}^-$ from diquarks

Zu-Hang Lin, Chun-Sheng An, and Cheng-Rong Deng\*

*School of Physical Science and Technology, Southwest University, Chongqing 400715, China*

We investigate the  $P$ -wave states  $T_{bb}^-$  in the isospin singlet and three excited modes [excitation occurring in the diquark  $[bb]_{c_1}^{s_1}$  ( $\rho$ -mode), antidiquark  $[\bar{u}\bar{d}]_{c_2}^{s_2}$  ( $r$ -mode) or between them ( $\lambda$ -mode)] from diquarks in a quark model. We analyze the dynamical behaviors of the diquark  $[bb]_{c_1}^{s_1}$ , antidiquark  $[\bar{u}\bar{d}]_{c_2}^{s_2}$  and their correlations in the states  $T_{bb}^-$  by decomposing the interactions from various sources in the model. The absolute dominant color-spin configuration, more than 99%, in the  $\rho$ -mode with  $1^1P_1$  is  $[bb]_{\mathbf{3}}^0[\bar{u}\bar{d}]_{\mathbf{3}}^0$ . Its energy is lower by about 18 MeV than the threshold  $\bar{B}\bar{B}$  so that it can establish a compact bound state. The chromomagnetic and meson-exchange interactions in the antidiquark  $[\bar{u}\bar{d}]_{\mathbf{3}}^0$  are responsible for its binding mechanism. Two other excited modes are higher than their respective threshold. The color configuration  $\mathbf{6} \otimes \bar{\mathbf{6}}$  need to be handled discreetly in the tetraquark states.

## I. INTRODUCTION

Searching for multi-quark hadrons is an extremely significant topic in hadronic physics because they may contain more abundant low-energy strong interaction information than ordinary hadrons. Theoretical explorations on the possible stable doubly heavy tetraquark states can be traced back to the early 1980s [1, 2]. Their properties have been studied extensively in various theoretical frameworks in recent years [3, 4], in particular since the LHCb Collaboration reported the doubly charmed state  $T_{cc}^+$  with  $01^+$  in the  $D^0D^0\pi^+$  invariant mass spectrum [5, 6]. The doubly heavy tetraquark states are usually discussed as a diquark-antidiquark or meson-meson configuration. The former can establish a compact state while the latter can produce a relative loose molecular state [3, 4]. The tendency to form stable bound states is proportional to the mass ratio of heavy quark and light antiquark. The majority of the existing theoretical investigations mainly concentrate on the doubly heavy tetraquark ground states, which indicates that the state  $T_{bb}^-$  with  $01^+$  can establish a deep bound state though it has not been observed in experiments [3, 4]. In this case, its  $P$ -wave excited states are most likely to be stable against the strong interactions in the low excited states of the doubly heavy tetraquark states. Recently, the  $P$ -wave excited states  $T_{bb}^-$  were explored using the lattice QCD potential and Born-Oppenheimer approximation [7, 8], quark models [9, 10], and the QCD Laplace sum rule [11].

The concept of diquarks was first proposed by Gell-Mann in his pioneering work on quarks [12]. Subsequently, diquarks are usually regarded as an elementary constituent to explore the properties of hadrons and hadron-hadron interactions [13]. It seems that there exists some phenomenological evidence of the relevance of the diquarks in hadron physics [14, 15]. The sizes of diquarks are often ignored for simplicity in some calcu-

lations [13], just like the sizes of constituent quarks are neglected. In the constituent quark models, diquarks are not a pointlike fundamental object but a spatially extended object with various color-spin-isospin-orbit configurations, which makes the hadron world more fantastic.

The substructures of the diquarks usually affect the structures and properties of hadrons and the diquark correlations might be critical to the formation of multi-quark hadrons [16–18]. The doubly heavy tetraquark states can provide a clear diquark picture so that they are extremely beneficial to research the substructures, natures and correlations of diquarks. Inspired by the state  $T_{cc}^+$  reported by the LHCb Collaboration, the lattice QCD calculation on the channel  $DD^*$  with  $01^+$  indicated that its short-range attraction was related to the attractive diquark color-spin configuration  $[cc]_{\mathbf{3}}^0[\bar{u}\bar{d}]_{\mathbf{3}}^1$  [19]. Similar short-range attraction was also found in the channel  $\bar{B}\bar{B}^*$  with  $01^+$  [19].

In this work, we prepare to explore the natures and structures of the  $P$ -wave excited states  $T_{bb}^-$  in the isospin singlet and various excited modes from the perspective of diquarks. We decode the natures of the diquark  $[bb]_{c_1}^{s_1}$  and antidiquark  $[\bar{u}\bar{d}]_{c_2}^{s_2}$  and their correlations in the non-relativistic quark model. The model can well describe the nature of the state  $T_{cc}^+$  [20]. The motivation of this paper is to broaden our visions on the properties and structures of the excited states  $T_{bb}^-$  from the perspective of the phenomenological model. We anticipate providing some valuable information for the experimental establishment of the doubly heavy tetraquark states in the future.

This paper is organized as follows. After the Introduction, we give the details of the quark model in Sec. II. We show the wave functions of the states  $T_{bb}^-$  in Sec. III. We present the numerical results and discussions in Sec. IV. We list a brief summary in the last section.

## II. QUARK MODEL

At the hadron scale, QCD is highly nonperturbative due to the complicated infrared behavior of the non-

\*crdeng@swu.edu.cn

Abelian  $SU(3)$  gauge group. The calculations of hadron spectra and the hadron-hadron interaction directly from QCD are very difficult at present. A less rigorous approach, the QCD-inspired quark model, is a powerful implement in obtaining physical insight for these complicated strong interacting systems. The quark model is formulated under the assumption that the hadrons are color-singlet nonrelativistic bound states of constituent quarks with phenomenological effective masses and interactions. One expects the model dynamics to be governed by QCD. The perturbative effect is the well-known one-gluon-exchange (OGE) interaction. From the non-relativistic reduction of the OGE diagram in QCD for point-like quarks one gets

$$V_{ij}^{\text{oge}} = \frac{\alpha_s}{4} \boldsymbol{\lambda}_i^c \cdot \boldsymbol{\lambda}_j^c \left( \frac{1}{r_{ij}} - \frac{2\pi\delta(\mathbf{r}_{ij})\boldsymbol{\sigma}_i \cdot \boldsymbol{\sigma}_j}{3m_i m_j} \right), \quad (1)$$

where  $\boldsymbol{\lambda}_i^c$  and  $\boldsymbol{\sigma}_i$  stand for the color  $SU(3)$  Gell-Mann matrices and spin  $SU(2)$  Pauli matrices, respectively.  $r_{ij}$  is the distance between the quarks  $i$  and  $j$  and  $m_i$  is the mass of the  $i$ -th quark. The Dirac  $\delta(\mathbf{r}_{ij})$  function should be regularized in the form [21]

$$\delta(\mathbf{r}_{ij}) \rightarrow \frac{1}{4\pi r_{ij} r_0^2(\mu_{ij})} e^{-\frac{r_{ij}}{r_0(\mu_{ij})}}, \quad (2)$$

where  $r_0(\mu_{ij}) = \frac{\hat{r}_0}{\mu_{ij}}$ ,  $\mu_{ij}$  is the reduced mass of two interacting particles  $i$  and  $j$ . The quark-gluon coupling constant  $\alpha_s$  adopts an effective scale-dependent form,

$$\alpha_s(\mu_{ij}^2) = \frac{\alpha_0}{\ln \frac{\mu_{ij}^2}{\Lambda_0^2}}, \quad (3)$$

$\hat{r}_0$ ,  $\Lambda_0$  and  $\alpha_0$  are adjustable parameters fixed by fitting the ground state meson spectrum.

The constituent quark mass originates from the breaking of the  $SU(3)_L \otimes SU(3)_R$  chiral symmetry at some momentum scale [22]. The chiral symmetry is spontaneously broken in the light quark sector while it is explicitly broken in the heavy quark sector. Once the light constituent quark mass is generated, it has to interact through Goldstone bosons  $\pi$ ,  $K$  and  $\eta$ . In addition, the scalar meson  $\sigma$  exchange interaction is involved. The explicit Goldstone boson exchange potentials  $V_{ij}^\pi$ ,  $V_{ij}^K$ ,  $V_{ij}^\eta$  and  $\sigma$ -meson exchange potential  $V_{ij}^\sigma$  are taken from Ref. [21],

$$\begin{aligned} V_{ij}^{\text{obe}} &= V_{ij}^\pi \sum_{k=1}^3 \mathbf{F}_i^k \mathbf{F}_j^k + V_{ij}^K \sum_{k=4}^7 \mathbf{F}_i^k \mathbf{F}_j^k \\ &\quad + V_{ij}^\eta (\mathbf{F}_i^8 \mathbf{F}_j^8 \cos \theta_P - \sin \theta_P), \\ V_{ij}^\chi &= \frac{g_{ch}^2}{4\pi} \frac{m_\chi^3}{12m_i m_j} \frac{\Lambda_\chi^2}{\Lambda_\chi^2 - m_\chi^2} \boldsymbol{\sigma}_i \cdot \boldsymbol{\sigma}_j \\ &\quad \times \left( Y(m_\chi r_{ij}) - \frac{\Lambda_\chi^3}{m_\chi^3} Y(\Lambda_\chi r_{ij}) \right), \quad Y(x) = \frac{e^{-x}}{x} \\ V_{ij}^\sigma &= -\frac{g_{ch}^2}{4\pi} \frac{\Lambda_\sigma^2 m_\sigma}{\Lambda_\sigma^2 - m_\sigma^2} \left( Y(m_\sigma r_{ij}) - \frac{\Lambda_\sigma}{m_\sigma} Y(\Lambda_\sigma r_{ij}) \right). \end{aligned} \quad (4)$$

$\mathbf{F}_i$  are the flavor  $SU(3)$  Gell-Mann matrices and  $\chi$  represents  $\pi$ ,  $K$  and  $\eta$ . The mass parameters  $m_\chi$  take their experimental values, while the cutoff parameters  $\Lambda_\chi$  and the mixing angles  $\theta_P$  take the values from [21]. The mass parameter  $m_\sigma$  can be determined through the partial conservation of axial vector current relation  $m_\sigma^2 \approx m_\pi^2 + 4m_{u,d}^2$  [23]. The chiral coupling constant  $g_{ch}$  can be obtained from the  $\pi NN$  coupling constant through

$$\frac{g_{ch}^2}{4\pi} = \left( \frac{3}{5} \right)^2 \frac{g_{\pi NN}^2}{4\pi} \frac{m_{u,d}^2}{m_N^2}. \quad (5)$$

In addition to the meson-exchange interactions, the quark model also incorporates another nonperturbative effect, color confinement, because observed hadrons in experiments are color singlets. However, it is still impossible to directly derive color confinement analytically from its QCD Lagrangian so far. From the perspective of phenomenology, quark confinement potential should only emerge from a model in which the interaction depends on color charges. In addition, the coupling between color charges increases with increasing separation. Quark confinement potential in the quark model can be generally manmade based on the two ingredients. In this work, the quark confinement potential can be written as

$$V_{ij}^{\text{con}} = -a_c \boldsymbol{\lambda}_i^c \cdot \boldsymbol{\lambda}_j^c r_{ij}^2. \quad (6)$$

To sum up, the complete Hamiltonian of the quark model for the mesons and  $T_{bb}^-$  can be presented as

$$\begin{aligned} H_n &= \sum_{i=1}^n \left( m_i + \frac{\mathbf{p}_i^2}{2m_i} \right) - T_c + \sum_{i<j}^n V_{ij} \\ V_{ij} &= V_{ij}^{\text{oge}} + V_{ij}^{\text{con}} + V_{ij}^{\text{obe}} + V_{ij}^\sigma, \end{aligned} \quad (7)$$

where  $\mathbf{p}_i$  is the momentum of the  $i$ -th quark and  $T_c$  is the center-of-mass kinetic energy. Accurately solving the two-body Schrödinger equation, we can obtain a set of model parameters by fitting the ground state meson spectrum with the Minit program [24], which are presented in Tables I and II, respectively.

### III. WAVE FUNCTIONS

In the diquark configuration, the Jacobi coordinates of the states  $T_{bb}^-$  are presented in Fig. 1. Their specific expressions can be written as

$$\begin{aligned} \boldsymbol{\rho} &= \mathbf{r}_1 - \mathbf{r}_2, \quad \mathbf{r} = \mathbf{r}_3 - \mathbf{r}_4, \\ \boldsymbol{\lambda} &= \frac{m_1 \mathbf{r}_1 + m_2 \mathbf{r}_2}{m_1 + m_2} - \frac{m_3 \mathbf{r}_3 + m_4 \mathbf{r}_4}{m_3 + m_4}, \end{aligned} \quad (8)$$

where  $\mathbf{r}_i$  stand for the position of the  $i$ -th particle in the states  $T_{bb}^-$ . Note that the coordinates are just a possible choice of many possibilities, which is most propitious to describe the natures of diquarks and their correlations.

TABLE I: Adjustable model parameters, quark mass and  $\Lambda_0$  unit in MeV,  $a_c$  unit in MeV·fm<sup>-2</sup>,  $r_0$  unit in MeV·fm and  $\alpha_0$  is dimensionless.

Para.	$m_{u,d}$	$m_s$	$m_c$	$m_b$	$a_c$	$\alpha_0$	$\Lambda_0$	$r_0$
Valu.	280	512	1602	4936	40.78	4.55	9.17	35.06

TABLE II: Ground state meson spectrum, units in MeV.

State	$\pi$	$\rho$	$\omega$	$K$	$K^*$	$\phi$	$D^\pm$
Theo.	142	826	780	492	974	1112	1867
PDG.	139	775	783	496	896	1020	1869
State	$D^*$	$D_s$	$D_s^*$	$\eta_c$	$J/\Psi$	$B$	$B^*$
Theo.	2002	1972	2140	2912	3102	5251	5301
PDG.	2007	1968	2112	2980	3097	5280	5325
State	$B_s$	$B_s^*$	$B_c$	$\eta_b$	$\Upsilon(1S)$		
Theo.	5377	5430	6261	9441	9546		
PDG.	5366	5416	6275	9391	9460		

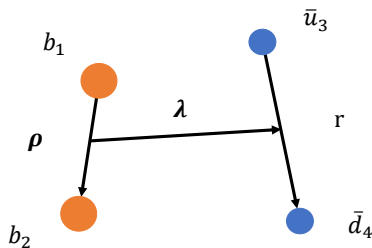


FIG. 1: Jacobi coordinates of the states  $T_{bb}^-$ . Orange balls stand for  $b$ -quarks and blue balls represent  $u$ - and  $d$ -quark.

The orbital angular momentum associated with those coordinates is denoted as  $l_\rho$ ,  $l_r$ , and  $l_\lambda$ , respectively. In the present work, we mainly concentrate on the  $P$ -wave excited states  $T_{bb}^-$ . The single  $P$ -wave excitation can take place in the diquark  $[bb]_{c_1}^{s_1}$  ( $\rho$ -mode:  $l_\rho = 1$ ), antiquark  $[\bar{u}\bar{d}]_{c_2}^{s_2}$  ( $r$ -mode:  $l_r = 1$ ), or between the diquark  $[bb]_{c_1}^{s_1}$  and antiquark  $[\bar{u}\bar{d}]_{c_2}^{s_2}$  ( $\lambda$ -mode:  $l_\lambda = 1$ ). Similar orbital excited modes were adopted to study the doubly heavy tetraquark states [9].

Accurate numerical calculations are a primary requirement to exactly comprehend the natures of the states  $T_{bb}^-$ . The Gaussian expansion method (GEM) has been proven to be rather powerful to solve the few-body problem in nuclear physics [25]. A recent comparative study revealed the superiority of the GEM over the resonating group method and the diffusion Monte Carlo method for the tetraquark bound states in quark models [26]. According to the GEM, the relative motion wave functions  $\phi_{lm}(\mathbf{x})$  can be expanded as the superpositions of a set of Gaussian functions with different sizes,

$$\phi_{lm}(\mathbf{x}) = \sum_{n=1}^{n_{max}} c_n N_n x^n e^{-\nu_n x^2} Y_{lm}(\hat{\mathbf{x}}), \quad (9)$$

where  $\mathbf{x}$  represents  $\boldsymbol{\rho}$ ,  $\mathbf{r}$  and  $\boldsymbol{\lambda}$ . More details about the GEM can be found in Ref. [25].

The color-spin configurations of the states  $T_{bb}^-$  can be denoted as  $[bb]_{c_1}^{s_1}[\bar{u}\bar{d}]_{c_2}^{s_2}$ , where the subscripts  $c_i$  and superscripts  $s_i$  are the color and spin, respectively. Both the diquark  $[bb]_{c_1}^{s_1}$  and antiquark  $[\bar{u}\bar{d}]_{c_2}^{s_2}$  can be in the spin singlet or triplet. The diquark  $[bb]_{c_1}^{s_1}$  is an isospin singlet and the antiquark  $[\bar{u}\bar{d}]_{c_2}^{s_2}$  can be in the isospin singlet or triplet similar to its spin. The color representations of the diquark  $[bb]_{c_1}^{s_1}$  can be antisymmetric  $\bar{\mathbf{3}}$  and symmetric  $\mathbf{6}$ . Those of the antiquark  $[\bar{u}\bar{d}]_{c_2}^{s_2}$  can be antisymmetric  $\mathbf{3}$  and symmetric  $\bar{\mathbf{6}}$ . The color configuration of the tetraquark state  $[bb][\bar{u}\bar{d}]$  can be written as

$$(\bar{\mathbf{3}} \oplus \mathbf{6}) \otimes (\mathbf{3} \oplus \bar{\mathbf{6}}) = \underbrace{(\bar{\mathbf{3}} \otimes \mathbf{3})}_{\mathbf{1} \oplus \mathbf{8}} \oplus \underbrace{(\bar{\mathbf{3}} \otimes \bar{\mathbf{6}})}_{\mathbf{8} \oplus \mathbf{10}} \oplus \underbrace{(\mathbf{6} \otimes \mathbf{3})}_{\mathbf{8} \oplus \mathbf{10}} \oplus \underbrace{(\mathbf{6} \otimes \bar{\mathbf{6}})}_{\mathbf{1} \oplus \mathbf{8} \oplus \mathbf{27}}$$

According to the colorless requirement, only two coupling modes,  $\bar{\mathbf{3}} \otimes \mathbf{3}$  and  $\mathbf{6} \otimes \bar{\mathbf{6}}$ , are permitted. In general, the physical state should be the mixture of those two color coupling modes.

The diquark  $[bb]_{c_1}^{s_1}$  and antiquark  $[\bar{u}\bar{d}]_{c_2}^{s_2}$  are a spatially extended compound with various color-spin-isospin-orbit configurations. Taking all degrees of freedom of identical particles into account, the Pauli principle imposes some restrictions on the quantum numbers of the diquark  $[bb]_{c_1}^{s_1}$  and antiquark  $[\bar{u}\bar{d}]_{c_2}^{s_2}$  [27]. The total wave function of the states  $T_{bb}^-$  with the isospin  $I$  and angular momentum  $J$  can be constructed as a sum of the following direct products of the diquark  $[bb]_{c_1}^{s_1}$ , antiquark  $[\bar{u}\bar{d}]_{c_2}^{s_2}$ , and their relative motion wave function  $\phi_{l_\lambda m_\lambda}(\boldsymbol{\lambda})$ ,

$$\Phi_{IJ}^{T_{bb}^-} = \sum_{\alpha} c_{\alpha} \left[ \Psi_{i_1 j_1 c_1 l_\rho}^{[bb]} \Psi_{i_2 j_2 c_2 l_r}^{[\bar{u}\bar{d}]} \phi_{l_\lambda m_\lambda}(\boldsymbol{\lambda}) \right]_{IJ}^{T_{bb}^-}. \quad (10)$$

The summation index  $\alpha$  represents all of the possible color-spin-isospin-orbit combinations that can be coupled into the total spin and isospin and the coefficients  $c_{\alpha}$  are determined by the model dynamics.

#### IV. NUMERICAL RESULTS AND ANALYSIS

We mainly concentrate on the natures of the  $P$ -wave excited states  $T_{bb}^-$  in the isospin singlet and three excited modes, which are listed in Tables III and IV. In order to exhibit the influences of the  $P$ -wave excitation on the states, we also present the natures of the ground state  $T_{bb}^-$  with  $1^3S_1$ . By accurately solving the four-body Schrödinger equation with the well-defined trial wave function, we can arrive at their eigenenergy and eigenwave function. Using the eigenwave function, we can calculate various energy distributions in the diquark  $[bb]_{c_1}^{s_1}$ , antiquark  $[\bar{u}\bar{d}]_{c_2}^{s_2}$  and between them in the states  $T_{bb}^-$ , which are listed in Table III. Subsequently, we can achieve their binding energy,  $\Delta E = E_4 - M_{b\bar{u}} - M_{b\bar{d}}$ , and

TABLE III: Various energy distribution in the diquark  $[bb]_{c_1}^{s_1}$ , antidiquark  $[\bar{u}\bar{d}]_{c_2}^{s_2}$  and between them ( $[bb]_{c_1}^{s_1}-[\bar{u}\bar{d}]_{c_2}^{s_2}$ ) in the states  $T_{bb}^-$ , unit in MeV. The superscripts  $\rho$ ,  $r$  and  $\lambda$  denote that the  $P$ -wave excitation occurs in the  $[bb]_{c_1}^{s_1}$ ,  $[\bar{u}\bar{d}]_{c_2}^{s_2}$  and between them, respectively.  $T$ ,  $V^{\text{con}}$ ,  $V^{\text{coul}}$ ,  $V^{\text{cm}}$ ,  $V^\sigma$ ,  $V^\pi$ , and  $V^\eta$  are the kinetic energy, confinement, Coulomb, chromomagnetic,  $\sigma$ -,  $\pi$ -, and  $\eta$ -meson-exchange, respectively.

$n^{2S+1}L_J$	Parts	$T$	$V^{\text{con}}$	$V^{\text{cm}}$	$V^{\text{coul}}$	$V^\eta$	$V^\pi$	$V^\sigma$	Parts	$T$	$V^{\text{con}}$	$V^{\text{cm}}$	$V^{\text{coul}}$	$V^\eta$	$V^\pi$	$V^\sigma$
$1^3S_1$	$[bb]_{\mathbf{3}}^{\frac{1}{2}}$	124	16	1	-199	0	0	0	$[bb]_{\mathbf{6}}^0$	51	-19	1	59	0	0	0
	$[\bar{u}\bar{d}]_{\mathbf{3}}^0$	789	55	-289	-257	57	-335	-40	$[\bar{u}\bar{d}]_{\mathbf{6}}^1$	249	-70	-10	68	-2	20	-14
	$[bb]_{\mathbf{3}}^{\frac{1}{2}}-[\bar{u}\bar{d}]_{\mathbf{3}}^0$	210	124	-2	-340	0	0	0	$[bb]_{\mathbf{6}}^0-[\bar{u}\bar{d}]_{\mathbf{6}}^1$	303	372	0	-764	0	0	0
$1^3P_{0,1,2}^\lambda$	$[bb]_{\mathbf{3}}^{\frac{1}{2}}$	115	18	1	-193	0	0	0	$[bb]_{\mathbf{6}}^0$	41	-24	1	52	0	0	0
	$[\bar{u}\bar{d}]_{\mathbf{3}}^0$	739	59	-273	-250	53	-316	-38	$[\bar{u}\bar{d}]_{\mathbf{6}}^1$	203	-85	-7	60	-1	14	-11
	$[bb]_{\mathbf{3}}^{\frac{1}{2}}-[\bar{u}\bar{d}]_{\mathbf{3}}^0$	282	216	-1	-232	0	0	0	$[bb]_{\mathbf{6}}^0-[\bar{u}\bar{d}]_{\mathbf{6}}^1$	449	552	0	-604	0	0	0
$1^1P_1^\rho$	$[bb]_{\mathbf{3}}^0$	138	39	0	-107	0	0	0	$[bb]_{\mathbf{6}}^1$	97	-28	-7	44	0	0	0
	$[\bar{u}\bar{d}]_{\mathbf{3}}^0$	775	55	-283	-253	56	-328	-40	$[\bar{u}\bar{d}]_{\mathbf{6}}^1$	248	-70	-10	68	-2	20	-14
	$[bb]_{\mathbf{3}}^0-[\bar{u}\bar{d}]_{\mathbf{3}}^0$	200	140	-4	-320	0	0	0	$[bb]_{\mathbf{6}}^1-[\bar{u}\bar{d}]_{\mathbf{6}}^1$	302	396	-24	-740	0	0	0
$1^1P_1^r$	$[bb]_{\mathbf{3}}^{\frac{1}{2}}$	116	17	1	-195	0	0	0	$[bb]_{\mathbf{6}}^0$	41	-24	0	50	0	0	0
	$[\bar{u}\bar{d}]_{\mathbf{3}}^1$	435	218	4	-93	1	2	-5	$[\bar{u}\bar{d}]_{\mathbf{6}}^0$	375	-125	4	42	-1	-5	-4
	$[bb]_{\mathbf{3}}^{\frac{1}{2}}-[\bar{u}\bar{d}]_{\mathbf{3}}^1$	165	228	-6	-240	0	0	0	$[bb]_{\mathbf{6}}^0-[\bar{u}\bar{d}]_{\mathbf{6}}^0$	257	552	-2	-596	0	0	0

TABLE IV: Binding energy  $\Delta E$  and the contribution from various interactions and kinetic energy to  $\Delta E$ , unit in MeV.  $\langle\rho^2\rangle^{\frac{1}{2}}$  and  $\langle\mathbf{r}^2\rangle^{\frac{1}{2}}$  are the size of the diquark  $[bb]_{c_1}^{s_1}$  and antidiquark  $[\bar{u}\bar{d}]_{c_2}^{s_2}$ , respectively, and  $\langle\lambda^2\rangle^{\frac{1}{2}}$  is their distance, unit in fm.

$n^{2S+1}L_J$	Color-spin, ratio	$\Delta E$	$\Delta T$	$\Delta V^{\text{con}}$	$\Delta V^{\text{cm}}$	$\Delta V^{\text{coul}}$	$\Delta V^\eta$	$\Delta V^\pi$	$\Delta V^\sigma$	$\langle\rho^2\rangle^{\frac{1}{2}}$	$\langle\mathbf{r}^2\rangle^{\frac{1}{2}}$	$\langle\lambda^2\rangle^{\frac{1}{2}}$
$1^3S_1$	$[bb]_{\mathbf{3}}^{\frac{1}{2}}[\bar{u}\bar{d}]_{\mathbf{3}}^0$ , >99%	-215	479	-50	-259	-67	57	-335	-40	0.39	0.71	0.64
	$[bb]_{\mathbf{6}}^0[\bar{u}\bar{d}]_{\mathbf{6}}^1$ , <1%	119	-38	40	94	19	-2	20	-14	0.60	1.13	0.53
	Mixing	-216	481	-51	-260	-68	57	-335	-40	0.39	0.71	0.64
$1^3P_{0,1,2}^\lambda$	$[bb]_{\mathbf{3}}^{\frac{1}{2}}[\bar{u}\bar{d}]_{\mathbf{3}}^0$ , >99%	55	494	49	-243	56	53	-316	-38	0.40	0.74	0.91
	$[bb]_{\mathbf{6}}^0[\bar{u}\bar{d}]_{\mathbf{6}}^1$ , <1%	511	51	199	22	237	-1	14	-11	0.67	1.25	0.72
	Mixing	55	494	49	-243	56	53	-316	-38	0.40	0.74	0.90
$1^1P_1^\rho$	$[bb]_{\mathbf{3}}^0[\bar{u}\bar{d}]_{\mathbf{3}}^0$ , >99%	-18	409	7	-210	91	56	-331	-40	0.60	0.72	0.65
	$[bb]_{\mathbf{6}}^1[\bar{u}\bar{d}]_{\mathbf{6}}^1$ , <1%	203	-53	69	39	144	-2	20	-14	0.72	1.13	0.53
	Mixing	-18	412	6	-213	89	56	-328	-40	0.60	0.72	0.65
$1^1P_1^r$	$[bb]_{\mathbf{3}}^{\frac{1}{2}}[\bar{u}\bar{d}]_{\mathbf{3}}^1$ , <1%	562	15	233	74	243	1	2	-5	0.40	1.42	0.71
	$[bb]_{\mathbf{6}}^0[\bar{u}\bar{d}]_{\mathbf{6}}^0$ , >99%	480	-30	176	80	265	-1	-5	-4	0.67	1.53	0.57
	Mixing	480	-28	176	78	265	-1	-5	-4	0.67	1.53	0.57

the contributions coming from each part of the Hamiltonian to  $\Delta E$  to show the underlying dynamic mechanism in detail, where  $E_4$  is the minimal eigenenergy and  $M_{b\bar{u}} + M_{b\bar{d}}$  is its lowest two-meson threshold. In addition, we calculate the average distances and the ratio of each color spin  $[bb]_{c_1}^{s_1}[\bar{u}\bar{d}]_{c_2}^{s_2}$  in the coupled channels. We present those numerical results in Table IV.

### A. Ground state $T_{bb}^-$ with $1^3S_1$

The ground state  $T_{bb}^-$  with  $1^3S_1$  is composed of two possible color-spin configurations  $[bb]_{\mathbf{3}}^{\frac{1}{2}}[\bar{u}\bar{d}]_{\mathbf{3}}^0$  and  $[bb]_{\mathbf{6}}^0[\bar{u}\bar{d}]_{\mathbf{6}}^1$ .

The chromomagnetic interaction and meson-exchange interactions in the antidiquark  $[\bar{u}\bar{d}]_{\mathbf{3}}^0$  can provide extremely strong attractions about 600 MeV, see Table III. The Coulomb interaction in the diquark  $[bb]_{\mathbf{3}}^{\frac{1}{2}}$  and antidiquark  $[\bar{u}\bar{d}]_{\mathbf{3}}^0$  also gives strong attractions. These strong attractions are beneficial to establish the deeply compact bound state  $T_{bb}^-$  with  $1^3S_1$  because they do not appear in the threshold  $\bar{B}\bar{B}^*$ . In strong contrast, those attractions in the diquark  $[bb]_{\mathbf{6}}^0$  and antidiquark  $[\bar{u}\bar{d}]_{\mathbf{6}}^1$  are very weak even repulsive, see Table III. Moreover, the color-electric interaction, i.e. confinement potential plus Coulomb interaction, between the diquark  $[bb]_{\mathbf{6}}^0$  and antidiquark  $[\bar{u}\bar{d}]_{\mathbf{6}}^1$  is much stronger than that between the

diquark  $[bb]_{\mathbf{3}}^1$  and antiquark  $[\bar{u}\bar{d}]_{\mathbf{3}}^0$ . The color-electric interaction between two colored subclusters in the color configurations  $\mathbf{3} \otimes \mathbf{3}$  and  $\mathbf{6} \otimes \mathbf{6}$  has been discussed in detail in Refs. [28, 29]. On the whole, the mass of the configuration  $[bb]_{\mathbf{3}}^1[\bar{u}\bar{d}]_{\mathbf{3}}^0$  is much lower, about 334 MeV, than that of the configuration  $[bb]_{\mathbf{6}}^0[\bar{u}\bar{d}]_{\mathbf{6}}^1$ . In fact, the relative strength of those interactions is also revealed by the average distances in Table IV. The stronger those interactions, the shorter the distances.

The color-spin configuration  $[bb]_{\mathbf{3}}^1[\bar{u}\bar{d}]_{\mathbf{3}}^0$  has a binding energy around  $-215$  MeV in comparison to the threshold  $\bar{B}\bar{B}^*$ , see Table IV. In principle, the ground state  $T_{bb}^-$  should be the mixture of the two color-spin configurations. After their channel coupling calculation, the binding energy of the state reduces to  $-216$  MeV so that the state is a deeply compact bound state, which is in good agreement with the conclusions of recent lattice calculations [30–33]. The color-spin configuration  $[bb]_{\mathbf{3}}^1[\bar{u}\bar{d}]_{\mathbf{3}}^0$  absolutely predominates the properties of the ground state while the color-spin configuration  $[bb]_{\mathbf{6}}^0[\bar{u}\bar{d}]_{\mathbf{6}}^1$  can be completely ignored, which is completely consistent with the conclusion in Ref. [34]. The vast majority of the binding energy comes from the chromomagnetic interaction and meson-exchange interactions in the antiquark  $[\bar{u}\bar{d}]_{\mathbf{3}}^0$ . In addition, the color-electric interaction also contributes an attraction about 120 MeV to the binding energy. The kinetic energy provides a strong repulsion, which is an obvious obstacle to forming this bound state.

In our previous work, see case (b) in Ref. [20], we obtained a relative loose molecular state  $T_{bb}^-$  with  $01^+$  using the same model Hamiltonian and parameters, where the binding mechanism is the weak residual interaction between two colorless mesons. Combining with the present work, the state  $T_{bb}^-$  with  $01^+$  can simultaneously exist in two different structures in the same model, which also takes place in the similar model study of the state [35]. The phenomenon was deemed as a hadronic analog of cluster formation in spectra of light nuclei, where cluster structures made of  $\alpha$  particles are developed around the  $\alpha$  emission thresholds, while the lower bound states are compact shell-model-like states [35]. We discussed the correlation between two structures based on the angular momentum algebra and thought that their difference comes from the different model spaces induced by different orbit excited modes [27].

### B. P-wave states $T_{bb}^-$ with $1^3P_{0,1,2}^\lambda$

In the excited states, the orbital excitation occurs between the diquark  $[bb]_{c_1}^{s_1}$  and antiquark  $[\bar{u}\bar{d}]_{c_2}^{s_2}$  so that their color-spin configurations are exactly the same with those of the ground state  $T_{bb}^-$  with  $^3S_1$ , see Table III. In this calculation, we do not introduce spin-orbit interaction and thus the states  $1^3P_{0,1,2}^\lambda$  are degenerate. We expect that mass differences among the states will be tiny since the differences are suppressed by the heavy quarks. The natures of the diquark  $[bb]_{c_1}^{s_1}$  and anti-

quark  $[\bar{u}\bar{d}]_{c_2}^{s_2}$  do not obviously change in the excited state  $T_{bb}^-$  in comparison to the ground state  $T_{bb}^-$ . However, the color-electric interactions between the diquark  $[bb]_{c_1}^{s_1}$  and antiquark  $[\bar{u}\bar{d}]_{c_2}^{s_2}$  increase significantly, which remarkably elevates the energy of the  $P$ -wave excited state  $T_{bb}^-$  with  $1^3P_{0,1,2}^\lambda$  relative to the ground state.

The mass of the color-spin configuration  $[bb]_{\mathbf{3}}^1[\bar{u}\bar{d}]_{\mathbf{3}}^0$  is much lower by about 450 MeV than that of the color-spin configuration  $[bb]_{\mathbf{6}}^0[\bar{u}\bar{d}]_{\mathbf{6}}^1$  because of their extremely different meson-exchange and chromomagnetic interactions between the antiquarks  $[\bar{u}\bar{d}]_{\mathbf{3}}^0$  and  $[\bar{u}\bar{d}]_{\mathbf{6}}^1$ . The channel coupling calculation indicates that the color-spin configuration  $[bb]_{\mathbf{3}}^1[\bar{u}\bar{d}]_{\mathbf{3}}^0$  completely dominates the natures of the excited states  $T_{bb}^-$  with  $1^3P_{0,1,2}^\lambda$ . Their masses are 55 MeV higher than its threshold  $\bar{B}\bar{B}^*$ , the main reason being that the  $P$ -wave excitation between the diquark  $[bb]_{\mathbf{3}}^1$  and the antiquark  $[\bar{u}\bar{d}]_{\mathbf{3}}^0$  enhances the color-electric interaction.

### C. P-wave state $T_{bb}^-$ with $1^1P_1^\rho$

In the excited state, the orbital excitation takes place in the diquark  $[bb]_{c_1}^{s_1}$ . The state consists of two color-spin configurations  $[bb]_{\mathbf{3}}^0[\bar{u}\bar{d}]_{\mathbf{3}}^0$  and  $[bb]_{\mathbf{6}}^1[\bar{u}\bar{d}]_{\mathbf{6}}^1$ . The properties of the antiquark  $[\bar{u}\bar{d}]_{c_2}^{s_2}$  in the state are almost exactly consistent with those in the ground state  $T_{bb}^-$  and the correlation between the diquark  $[bb]_{c_1}^{s_1}$  and antiquark  $[\bar{u}\bar{d}]_{c_2}^{s_2}$  just changes a little bit, see Table III. The Coulomb interaction in the antiquark  $[bb]_{\mathbf{3}}^0$  is reduced by about 92 MeV because the interaction is sensitive to the distance change induced by the  $P$ -wave excitation. Other natures of the diquark  $[bb]_{c_1}^{s_1}$  do not dramatically vary although its orbit is in the  $P$ -wave excitation because of the suppression of the large mass of  $b$ -quarks.

The dominant color-spin configuration of the state  $T_{bb}^-$  with  $1^1P_1^\rho$  is  $[bb]_{\mathbf{3}}^0[\bar{u}\bar{d}]_{\mathbf{3}}^0$ , in which the chromomagnetic and meson-exchange interactions in the antiquark  $[\bar{u}\bar{d}]_{\mathbf{3}}^0$  can still provide an extremely strong attraction. Relative to the threshold  $\bar{B}\bar{B}$ , the binding energy of the state is about  $-18$  MeV so that it can establish a compact bound state. Its binding mechanism originates from the chromomagnetic and meson-exchange interactions in the antiquark  $[\bar{u}\bar{d}]_{\mathbf{3}}^0$ , see Table IV. The color-electric interaction, especially for the Coulomb interaction, is not a binding mechanism anymore because of the  $P$ -wave excitation in the diquark  $[bb]_{\mathbf{3}}^0$ . The contributions from the Coulomb interaction in the excited state  $T_{bb}^-$  with  $1^1P_1^\rho$  and the ground state  $T_{bb}^-$  with  $^3S_1$  are the main reason resulting in their binding energy difference.

Bicudo *et al.* studied the state  $T_{bb}^-$  with  $01^-$ , where the  $P$ -wave excitation occurs in the diquark  $[bb]$ , using the lattice QCD potentials, Born-Oppenheimer approximation and emergent wave method [7]. Its mass is  $10576_{+4}^{-4}$  MeV, which is close to our prediction on the state but 16 MeV higher than the threshold  $\bar{B}\bar{B}$ . The state can

decay into two  $\bar{B}$  mesons via strong interaction so that it is a resonance. Subsequently, Hoffmann *et al.* refined the investigation of the state by including heavy quark spin effects via the mass difference between  $B$  and  $B^*$  mesons [8]. They did not find any indication for the existence of the resonance [8].

#### D. P-wave state $T_{bb}^-$ with $1^1P_1^-$

In the excited state, the orbital excitation occurs in the antiquark  $[\bar{u}\bar{d}]_{c_2}^{s_2}$ , which induces a huge impact on its natures relative to its ground state because of the changes of its spin and size, especially for the diquark  $[\bar{u}\bar{d}]_{\bar{3}}$ , see Table III. The meson-exchange and chromomagnetic interactions in the antiquark  $[\bar{u}\bar{d}]_{\bar{3}}$  are weak, just several MeVs, while they can provide strong attractions, around 600 MeV, in the antiquark  $[\bar{u}\bar{d}]_{\bar{3}}^0$ . In addition, the color-electric interaction in the antiquark  $[\bar{u}\bar{d}]_{\bar{3}}$  is much higher, about 320 MeV, than that in the antiquark  $[\bar{u}\bar{d}]_{\bar{3}}^0$ . Relatively speaking, the natures of the antiquark  $[\bar{u}\bar{d}]_{\bar{6}}^0$  do not dramatically vary in comparison to its ground state  $[\bar{u}\bar{d}]_{\bar{6}}^1$ .

The total mass of the antiquark  $[\bar{u}\bar{d}]_{\bar{3}}^1$  is about 280 MeV higher than that of the antiquark  $[\bar{u}\bar{d}]_{\bar{6}}^0$  mainly because of the color-electric interaction. The fact directly results in that the dominant color-spin configuration in the excited state is  $[bb]_{\bar{6}}^0[\bar{u}\bar{d}]_{\bar{6}}^0$  rather than  $[bb]_{\bar{3}}^1[\bar{u}\bar{d}]_{\bar{3}}^1$ . Therefore, the color configuration  $\mathbf{6}\otimes\bar{\mathbf{6}}$  should not be unhesitatingly discarded in the tetraquark excited states. The mass of the color-spin configuration  $[bb]_{\bar{6}}^0[\bar{u}\bar{d}]_{\bar{6}}^0$  is much higher, about 480 MeV, than its threshold  $\bar{B}\bar{B}$ , see Table IV. The chromomagnetic and color-electric interactions cannot provide any attractions. Furthermore, the meson-exchange interactions just give an attraction of 10 MeV. However, the kinetic energy contributes an attraction of about 30 MeV to the binding energy mainly because of the spatial extension of the diquark  $[bb]_{\bar{6}}^0$  and antiquark  $[\bar{u}\bar{d}]_{\bar{6}}^0$  due to the absence of strong binding forces in them. The channel coupling calculation of the two color-spin configurations does not change the mass of the state.

#### E. P-wave states $T_{bb}^-$ in other models

The  $P$ -wave states  $T_{bb}^-$  in the three excited modes were investigated in the potential chiral-diquark model [9]. The states  $T_{bb}^-$  were described as a threebody system composed of two heavy quarks and an antiquark only in the color configuration  $\bar{\mathbf{3}}\otimes\mathbf{3}$ . The  $P$ -wave excited states  $T_{bb}^-$  with  $0^-$ ,  $1^-$  and  $2^-$  in the excited  $\lambda$ -mode were investigated in a constituent quark model [10], where the four-body problem is solved in a variational method. None of the  $P$ -wave bound states  $T_{bb}^-$  can be found because their predicted masses are much farther away from their corresponding threshold [9, 10]. The predicted masses for

the  $01^-$  states in the  $\rho$ - and  $\lambda$ -mode are higher over 100 MeV higher than those of the present work because of the absence of meson exchange interactions providing strong attractions, which is held true for the ground state  $T_{bb}^-$  with  $01^+$ . The excited state with  $01^-$  in the  $\xi_P$ -mode is close to that in the  $r$ -mode of the present work because the meson exchange interaction is very weak [9].

The tetraquark states with diquark configuration include two color configurations  $\bar{\mathbf{3}}\otimes\mathbf{3}$  and  $\mathbf{6}\otimes\bar{\mathbf{6}}$ . The configuration  $\bar{\mathbf{3}}\otimes\mathbf{3}$  is usually preferred over the configuration  $\mathbf{6}\otimes\bar{\mathbf{6}}$  in the studies of tetraquark states with diquark configuration [15]. In fact, the configuration  $\mathbf{6}\otimes\bar{\mathbf{6}}$  plays an important role in some systems, such as the fully-heavy tetraquark states [29, 36, 37]. For the  $S$ -wave state  $T_{bb}^-$  with diquark configurations, its main configuration is widely regarded as  $\bar{\mathbf{3}}\otimes\mathbf{3}$  in various theoretical studies [3, 4], which is supported by the comparative research [27, 34]. For the  $P$ -wave states  $T_{bb}^-$  in the  $r$ -mode, the present comparative study indicates that the color configuration  $\mathbf{6}\otimes\bar{\mathbf{6}}$  instead of  $\bar{\mathbf{3}}\otimes\mathbf{3}$  is its dominant component [9]. In this way, the color configuration  $\mathbf{6}\otimes\bar{\mathbf{6}}$  needs to be handled discreetly in the tetraquark states.

## V. SUMMARY

We study the  $P$ -wave excited states  $T_{bb}^-$  in the isospin singlet and three excited modes from diquarks with the Gaussian expansion method in the quark model. We decode the dynamical natures of the diquark  $[bb]_{c_1}^{s_1}$ , antiquark  $[\bar{u}\bar{d}]_{c_2}^{s_2}$  and their correlations in the states  $T_{bb}^-$  by decomposing the interactions from various sources in the quark model. The ground state antiquark  $[\bar{u}\bar{d}]_{\bar{3}}^0$  can provide extremely strong attractions coming from meson-exchange, Coulomb, and chromomagnetic interactions. Those interactions in the antiquark  $[\bar{u}\bar{d}]_{c_2}^{s_2}$  with other quantum numbers are weak even repulsive. The Coulomb interaction predominates the natures of the diquark  $[bb]_{c_1}^{s_1}$ , especially  $[bb]_{\bar{3}}^1$  and  $[bb]_{\bar{3}}^0$  ( $P$ -wave), because the interaction is proportional to  $\frac{1}{r}$  and the large mass of  $b$ -quarks allows two  $b$ -quarks to be as close as possible. The correlations between the diquark  $[bb]_{c_1}^{s_1}$  and antiquark  $[\bar{u}\bar{d}]_{c_2}^{s_2}$  through the color-electric interaction only depend on the color representations of the states  $T_{bb}^-$ . Either in the ground state or in the  $P$ -wave states, the correlations in the color configuration  $\mathbf{6}\otimes\bar{\mathbf{6}}$  are stronger than those in the color configuration  $\bar{\mathbf{3}}\otimes\mathbf{3}$ .

The dominant color-spin configurations of the states  $T_{bb}^-$  with  ${}^3P_{0,1,2}^\lambda$  and  ${}^1P_1^\rho$  are  $[bb]_{\bar{3}}^1[\bar{u}\bar{d}]_{\bar{3}}^0$  and  $[bb]_{\bar{3}}^0[\bar{u}\bar{d}]_{\bar{3}}^0$ , respectively, which are more than 99%. In strong contrast, those of the state  $T_{bb}^-$  with  ${}^1P_1^r$  is  $[bb]_{\bar{6}}^0[\bar{u}\bar{d}]_{\bar{6}}^0$  instead of  $[bb]_{\bar{3}}^1[\bar{u}\bar{d}]_{\bar{3}}^1$ , which indicates that the color configuration  $\mathbf{6}\otimes\bar{\mathbf{6}}$  needs to be handled discreetly in the tetraquark states. The mass of the state with  ${}^1P_1^\rho$  is 18 lower MeV than the threshold  $\bar{B}\bar{B}$  so that it can form a compact bound state. The meson-exchange and chromomagnetic interactions in the antiquark  $[\bar{u}\bar{d}]_{\bar{3}}^0$  are responsible for

its binding mechanism. The masses of the other two excited modes are higher than their respective threshold so that they may be resonances.

The discovery of the state  $T_{cc}^+$  has opened a new window for the doubly heavy tetraquark states. The current study on the states  $T_{bb}^-$  may be beneficial to understand their underlying behaviors and nonperturbative QCD dynamics. We sincerely expect more theoretical and experimental investigations to inspect the tetraquark states from various perspectives in the near future.

## Acknowledgments

This research is supported by the Chongqing Natural Science Foundation under Project No. cstc2021jcyj-msxmX0078 and the Fundamental Research Funds for the Central Universities under Grant No. SWU-XDJH202304.

- 
- [1] J.P. Ader, J.M. Richard and P. Taxil, Phys. Rev. D **25**, 2370 (1982).
- [2] J.L. Ballot and J.M. Richard, Phys. Lett. B **123**, 449 (1983).
- [3] H.X. Huang, C.R. Deng, X.J. Liu, Y. Tan and J.L. Ping, Symmetry **15**, 1298 (2023).
- [4] H.X. Chen, W. Chen, X. Liu, Y.R. Liu and S.L. Zhu, Rept. Prog. Phys. **86**, 026201 (2023).
- [5] R. Aaij *et al.* [LHCb], Nature Phys. **18**, 751 (2022).
- [6] R. Aaij *et al.* [LHCb], Nature Commun. **13**, 3351 (2022).
- [7] P. Bicudo, M. Cardoso, A. Peters, M. Pflaumer and M. Wagner, Phys. Rev. D **96**, 054510 (2017).
- [8] J. Hoffmann, A. Zimmermann-Santos and M. Wagner, PoS **LATTICE2022**, 262 (2023).
- [9] Y. Kim, M. Oka and K. Suzuki, Phys. Rev. D **105**, 074021 (2022).
- [10] Q. Meng, M. Harada, E. Hiyama, A. Hosaka and M. Oka, Phys. Lett. B **824**, 136800 (2022).
- [11] R. Albuquerque, S. Narison and D. Rabetiarivony, Nucl. Phys. A **1034**, 122637 (2023).
- [12] M. Gell-Mann, Phys. Lett. **8**, 214 (1964).
- [13] M. Anselmino, E. Predazzi, S. Ekelin, S. Fredriksson and D.B. Lichtenberg, Rev. Mod. Phys. **65**, 1199 (1993).
- [14] R.L. Jaffe, Phys. Rept. **409**, 1 (2005).
- [15] M.Y. Barabanov, M.A. Bedolla, W.K. Brooks, G.D. Cates, C. Chen, Y. Chen, E. Cisbani, M. Ding, G. Eichmann and R. Ent, *et al.* Prog. Part. Nucl. Phys. **116**, 103835 (2021).
- [16] S.L. Olsen, T. Skwarnicki and D. Zieminska, Rev. Mod. Phys. **90**, 015003 (2018).
- [17] F.K. Guo, X.H. Liu and S. Sakai, Prog. Part. Nucl. Phys. **112**, 103757 (2020).
- [18] Y.R. Liu, H.X. Chen, W. Chen, X. Liu and S.L. Zhu, Prog. Part. Nucl. Phys. **107**, 237 (2019).
- [19] Y. Lyu, S. Aoki, T. Doi, T. Hatsuda, Y. Ikeda and J. Meng, Phys. Rev. Lett. **131**, 161901 (2023).
- [20] C.R. Deng and S.L. Zhu, Phys. Rev. D **105**, 054015 (2022).
- [21] J. Vijande, F. Fernandez and A. Valcarce, J. Phys. G **31**, 481 (2005).
- [22] A. Manohar and H. Georgi, Nucl. Phys. B **234**, 189 (1984).
- [23] M.D. Scadron, Phys. Rev. D **26**, 239 (1982).
- [24] F. James and M. Roos, Comput. Phys. Commun. **10**, 343 (1975).
- [25] E. Hiyama, Y. Kino and M. Kamimura, Prog. Part. Nucl. Phys. **51**, 223 (2003).
- [26] L. Meng, Y. K. Chen, Y. Ma and S.L. Zhu, Phys. Rev. D **108**, 114016 (2023).
- [27] C.R. Deng and S.L. Zhu, Sci. Bull. **67**, 1522 (2022).
- [28] Y.H. Wang, J. Wei, C.S. An and C.R. Deng, Chin. Phys. Lett. **40**, 021201 (2023).
- [29] C.R. Deng, H. Chen and J.L. Ping, Phys. Rev. D **103**, 014001 (2021).
- [30] A. Francis, R.J. Hudspith, R. Lewis and K. Maltman, Phys. Rev. Lett. **118**, 142001 (2017).
- [31] P. Junnarkar, N. Mathur and M. Padmanath, Phys. Rev. D **99**, 034507 (2019).
- [32] P. Mohanta and S. Basak, Phys. Rev. D **102**, 094516 (2020).
- [33] L. Leskovec, S. Meinel, M. Pflaumer and M. Wagner, Phys. Rev. D **100**, 014503 (2019).
- [34] Q. F. Lü, D. Y. Chen and Y. B. Dong, Phys. Rev. D **102**, 034012 (2020).
- [35] Q. Meng, E. Hiyama, A. Hosaka, M. Oka, P. Gubler, K.U. Can, T.T. Takahashi and H.S. Zong, Phys. Lett. B **814**, 136095 (2021).
- [36] G.J. Wang, L. Meng and S.L. Zhu, Phys. Rev. D **100**, 096013 (2019).
- [37] W.L. Wu, Y.K. Chen, L. Meng and S.L. Zhu, [arXiv: 2401.14899 [hep-ph]].